Energy and Buildings 86 (2015) 550–556

Contents lists available at ScienceDirect

Energy and Buildings

journal homepage: www.elsevier.com/locate/enbuild

An optimized crossflow plate-fin membrane-based total heat exchanger

Qiu Zhong, Liping Yang*, Ye Tao, Caiyun Luo, Zijun Xu, Tonggeng Xi

The Shanghai Institute of Ceramics, Chinese Academy of Sciences, No. 1295 Dingxi Load, 200050 Shanghai, China

ARTICLE INFO

Article history:
Received 16 June 2014
Received in revised form 16 October 2014
Accepted 18 October 2014
Available online 28 October 2014

Keywords:
Total heat exchanger
Experimental research
Finite element analysis
Modified structure
Heat exchange efficiency

ABSTRACT

In this paper, a test rig was constructed to measure the sensibility and enthalpy effectiveness of a plate-fin total heat exchanger (PFTHE). Combined with finite element method, the influence of airflow distribution was analyzed, and an improved PFTHE was subsequently introduced. Utilizing the test rig, the study measured the sensibility and enthalpy effectiveness of the improved PFTHEs with air deflectors and different air spreader plates. Results show that the sensibility and enthalpy effectiveness of the PFTHE are optimized at 17.4% and 7.8% airflow rates, respectively.

1. Introduction

At present, many engineering systems advocate the use of less energy while maintaining the same functions and exceeding the performance required by previously designed systems. This concept is especially true for heating, ventilating, and air conditioning (HVAC) systems. Buildings and their HVAC systems should be energy efficient while satisfying the ever-increasing demand for better indoor air quality, performance, and environmental preservation. Research shows that membrane-based total heat exchanger (MTHE) is an effective means to reduce the energy consumption of ventilation systems [1–3]. The MTHE allows ventilation systems to reduce energy consumption given the heat and moisture recovery of exhausted air of the buildings [4,5]. Literature indicates that that the MTHE is the most effective device for energy-saving, commercial/industrial buildings [6,7] and residence [8,9]. How to increase the effectiveness of heat and moisture exchanger has been the key issue in this field. Most studies focus on improving the intensification of heat and mass transfer. In the aspect of structure design of channel, the use of triangular plate-fin (PF) structure had significant improvement on heat transfer efficiency compared with the parallel plates [2,10]. Recent research shows that with corrugated plate-fin, the heat transfer was improved with little pressure-drop penalty compared to the triangular plate-fin [11]. In the other hand, the most effective mean to improve the efficiency is the utilization of novel membranes to enhance moisture and heat transfer. Different type membrane materials [12–15] was used in MTHE. The influence of properties [16,17], selective permeation [18], spacing and thickness [19] of the membrane were studied experimentally. The influence of adsorption heat, the moisture and thermal resistance of membrane were also studied theoretically [20–22]. Two excellent review articles were presented on recent membrane progress on HVAC by Woods and Zhang, respectively [23,24]. Some researchers have delved on the effects of flow arrangements by using quasi-counter flow design instead of the crossflow [25]. Noticeable advantages include high efficiency, ease of construction and no moving parts, has have made quasi-counter flow design of exchanger become a research hotspot [26–30]. However, it is still a long term for the use of this type exchanger in residential/commercial buildings.

The above researches mainly focuses on the core structure or membrane materials, whereas relatively limited attention has been devoted to the optimization of air channel of MTHE. In this study, we optimized crossflow PF MTHE with air deflector and air spreader plate. The performance of the optimized MTHEs was measured, hence indicated a significant improvement in the efficiency of heat exchange.

2. Classic exchanger

The crossflow with PF is the most commercial MTHE design in the market because of its simplicity and the ease of duct seal

* Corresponding author. Tel.: +86 21 5241 3405; fax: +86 21 5241 3406.
E-mail address: lpyang@mail.sic.ac.cn (L. Yang).

http://dx.doi.org/10.1016/j.enbuild.2014.10.036
0378-7788/

Nomenclature

Letters

c	air specific heat
C	concentration
D	mass diffusion coefficient
h	enthalpy
H	convective heat transfer coefficient
k	convective mass transfer coefficient
L	latent heat
M	cross-sectional mass transfer rate
m	average mass flow rate of air
N	nonuniform coefficient
S	humidity
T	temperature
v	velocity
δ	thickness of membrane
η	effectiveness
λ	heat conductivity coefficient of membrane
ρ	air density
U	uncertainty

subscript

e	exhaust air
f	flesh air
h	enthalpy
i	inlet air
j	flesh air flow direction (x) or exhaust air flow direction (y)
m	membrane
n	flesh in or flesh out
n	total number of channels
o	outlet air
s	latent
T	sensible
w	water

required for MTHE systems. Fig. 1 shows the crossflow PF MTHE design. The fresh air and exhaust air was injected in the MTHE. The core of MTHE will provide a crossflow arrangement, therefore, the heat and moisture transfer will occurred over the plate-fin and membrane. As a result, the amount of energy will be recovered.

2.1. Test rig

Test rig is used in measuring the steady state heat and moisture transfer through the THE by considering inlet and outlet temperatures, humidity, and airflow rates. The sensibility and the latent effectiveness are the performance indices. A schematic

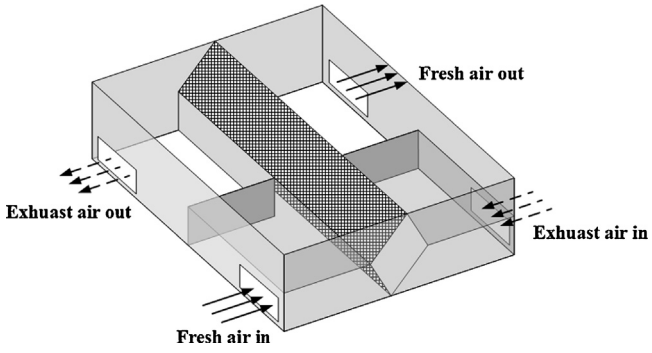

Fig. 1. Depiction of a crossflow PF MTHE design.

of the test rig is shown in Fig. 2. The rig is divided into three rooms, in which the left and the right rooms are intended for simulating outdoor and indoor conditions and comprised two 310 mm × 280 mm × 3000 mm ducts. With air conditioning and electric heating coils, the temperature and humidity can be controlled and maintained even under hot and humid ambient weather conditions. The exchanger in the middle room is connected to the ducting works with four inlet/outlet vents by flanges. Data of temperature/moisture, pressure, and air speed in the duct can be detected by different sensors. During the experiment, equal airflow rates are stored for the four ducts, which are changed from 300 m^3/h to 600 m^3/h by variable speed blowers to generate different air velocities. The airflow under such conditions is laminar, with Reynolds numbers not exceeding 8800. From these preparatory undertakings, the test rig is considered reliable. Heat and mass balance is a time-consuming process requiring more than 12 h to complete under one testing condition.

After measuring inlet and outlet temperature and humidity, the temperature, latent and enthalpy effectiveness are calculated by

$$\eta_T = \frac{T_{fo} - T_{fi}}{T_{eo} - T_{fi}} \quad \eta_s = \frac{S_{fo} - S_{fi}}{S_{eo} - S_{fi}} \quad \eta_h = \frac{h_{fo} - h_{fi}}{h_{eo} - h_{fi}} \tag{1}$$

where η_T, η_s, and η_h are the sensibility, latency, and enthalpy effectiveness, respectively; T is temperature; S is humidity; h is enthalpy; subscripts *fo*, *fi*, and *eo* refer to flesh out, flesh in, and exhaust out, respectively.

2.2. Uncertainty analysis

In the test rig, the accuracy of temperature sensor is ≤0.2 °C, the accuracy of moisture sensor is ≤2%. For 95% confidence interval, the uncertainty of three different temperature sensors are U_{Tfo} = 0.203 °C, U_{Tfi} = 0.204 °C, U_{Teo} = 0.206 °C and the uncertainty of three different moisture sensors are U_{sfo} = 0.038 g/kg, U_{sfi} = 0.036 g/kg, U_{seo} = 0.045 g/kg. Therefore, the uncertainty of enthalpy are U_{hfo} = 0.110 g/kg, U_{hfi} = 0.114 g/kg, U_{heo} = 0.149 g/kg.

Based on Eq. (1), the uncertainty of temperature, latent and sensibility effectiveness can be calculated by

$$\frac{U_X}{\eta_X} = \sqrt{\left(\frac{1}{X_{fo} - X_{fi}} \times U_{Tfo}\right)^2 + \left(-\frac{1}{X_{fo} - X_{fi}} \times U_{Tfi}\right)^2 + \left(-\frac{1}{X_{eo} - X_{fi}} \times U_{Teo}\right)^2} \tag{2}$$

where, X indicates temperature (T), latent (S) and sensibility(h) separately. Therefore, the uncertainty of sensibility effectiveness (U_T/η_T) is 7.73%, the uncertainty of latency effectiveness (U_S/η_s) is 5.19%, the uncertainty of enthalpy effectiveness (U_h/η_h) is 2.78%.

2.3. Mathematical control equation

To discuss further the experimental results, a physics model was constructed (Fig. 3). In which, the flesh airstream and exhaust airstream flow through in a cross-flow pattern. The model was formulated based on the following assumptions:

(1) Both the heat and the mass transfers are steady.
(2) The physical properties of the air fluid and membrane are constant.
(3) Heat conduction and vapor diffusion in the two airstreams in the directions parallel to the channel walls are negligible compared to the bulk convection.

According to Liu [3], with Peclet number (Pe) bigger than 2, the effect of axial air conduction/diffusion can be totally negligible. In our present work, with $Pe = Re \times Pr = c_{pa}\rho_a u d_e/\lambda_a = 7400$, the assumption (3) is valid. The mathematical control equations

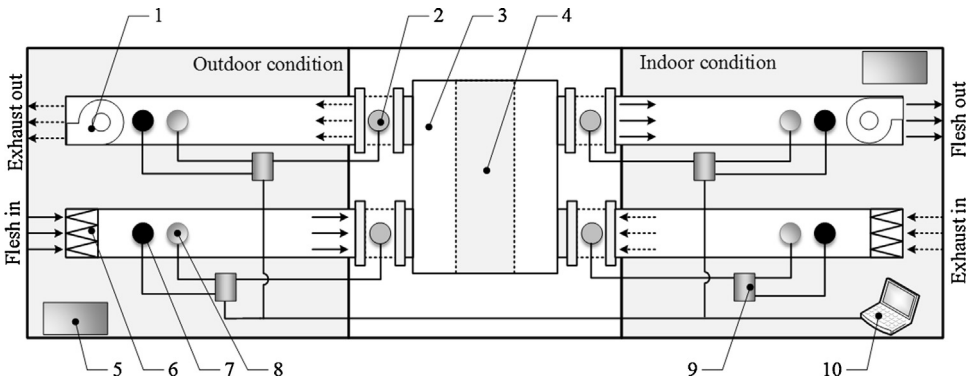

Fig. 2. Schematic of the test rig ((1) outlet blower; (2) temperature/moisture sensor; (3) exchanger; (4) core; (5) air-condition; (6) heater; (7) air speed sensor; (8) pressure sensor; (9) data acquisition unit; (10) computer).

for analyzing the coupled heat and mass transfer in MTHE can be described as follow [8], for flesh air,

$$\rho_f c_p \upsilon_f d\frac{\partial T_f}{\partial x} + 2H_f\left(T_f - T_{mf}\right) = 0 \tag{3}$$

$$\upsilon_f d\frac{\partial C_f}{\partial x} + 2k_f\left(C_f - C_{ms}\right) = 0 \tag{4}$$

For exhaust air,

$$\rho_e c_p \upsilon_e d\frac{\partial T_e}{\partial y} + 2H_e\left(T_e - T_{me}\right) = 0 \tag{5}$$

$$\upsilon_e d\frac{\partial C_e}{\partial y} + 2k_e\left(C_e - C_{me}\right) = 0 \tag{6}$$

On the membrane,

$$m_w c_{pw}\frac{\partial T_m}{\partial z} - \lambda_m\frac{\partial^2 T_m}{\partial x^2} - \lambda_m\frac{\partial^2 T_m}{\partial y^2} - \lambda_m\frac{\partial^2 T_m}{\partial z^2} = 0 \tag{7}$$

$$m_w = -D_{wm}\frac{\partial C}{\partial z} = D_{wm}\frac{C_f - C_e}{\delta} \tag{8}$$

where ρ is air density; υ is inlet air velocity; C is the water vapor density in the air-flow; T is temperature; c_p is air specific heat; H is convective heat transfer coefficient; k is convective mass transfer coefficient; λ is heat conductivity coefficient of membrane; m_w is moisture flow rate through membrane; D_{wm} is mass diffusion coefficient of steam in membrane; δ is thickness of membrane; subscript n indicates flesh in or flesh out; subscript f and e indicates fresh airflow or exhaust airflow; and subscript m indicates membrane.

With Eqs. (3)–(6), only the changes of the energy carried by the flesh and exhaust airstreams along their flow directions (x and y) through the heat and mass transfer across the membrane were reflected. They can be considered as boundary conditions for the heat and mass transfer within the membrane, which are controlled by Eqs. (7) and (8). Therefore, the boundary conditions are as follows, For flesh air,

$$T_s\big|_{x=0} = T_{si} \quad C_s\big|_{j=0} = C_{si} \tag{9}$$

For exhaust air,

$$T_e\big|_{y=0} = T_{ei} \quad C_e\big|_{y=0} = C_{ei} \tag{10}$$

On the membrane,

$$\left.\frac{\partial T_m}{\partial x}\right|_{x=0} = 0, \quad \left.\frac{\partial T_m}{\partial x}\right|_{x=xF} = 0, \quad \left.\frac{\partial T_m}{\partial y}\right|_{y=0} = 0, \quad \left.\frac{\partial T_m}{\partial y}\right|_{y=yF} = 0 \tag{11}$$

On the membrane surface of the flesh air,

$$-\lambda_m\left.\frac{\partial T_m}{\partial z}\right|_{z=0} = h_n\left(T_n - T_m\right) + m_w L_w \tag{12}$$

On the membrane surface of the exhaust air,

$$-\lambda_m\left.\frac{\partial T_m}{\partial z}\right|_{z=0} = h_n\left(T_n - T_m\right) + m_w L_w \tag{13}$$

where L_w is the latent heat of vaporization, and subscript i is inlet.

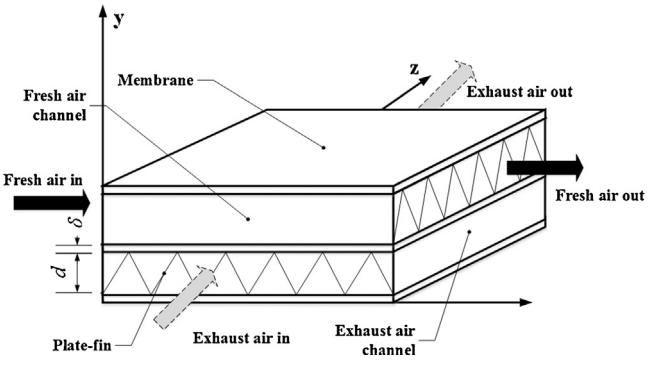

Fig. 3. Model of the exchanger core.

2.4. Results and discussion of the experiment

With the test rig, the latency and sensibility effectiveness of MTHE (Fig. 1) were measured; the flesh/exhaust inlet conditions are listed in Table 1. To discuss the influence of the construction of MTHE, the latency and sensibility effectiveness of MTHE with half windward (left half covered) of core were also measured. Results in Fig. 4 show that with the area of core windward decreasing by half, reduction was indicated as well with latent effectiveness at 2.3%, 3.9%, and 4.3% and with sensibility effectiveness at 3.2%, 4.6%, and 5.6% at 400, 500, and 600 m^3/h, separately.

Thus, we note the following: (1) As the area of MTHE core windward is halved, the latency and the sensibility effectiveness reduced only at approximately 5%. Therefore, the area of MTHE core for temperature and moisture exchange was not effectively used, especially the covered area of the core. (2) The latency drop and the

Table 1
Experimental conditions.

Exhaust inlet (indoor)		Flesh inlet (outdoor)	
T (°C)	Moisture (g/kg)	T (°C)	Moisture (g/kg)
21.5 ± 0.5	9.5 ± 0.5	13.5 ± 0.5	5.8 ± 0.5

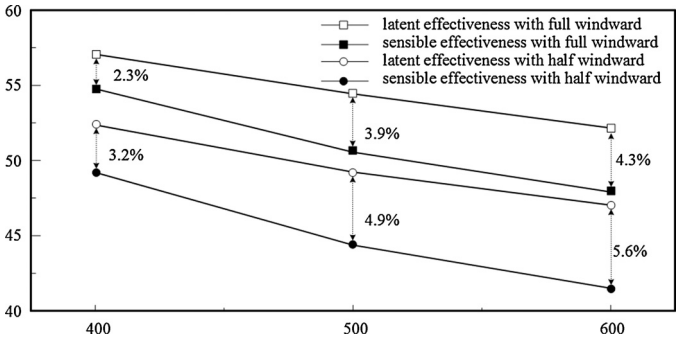

Fig. 4. Latency and sensibility effectiveness of MTHE with full/half windward.

Table 2
Parameters used in finite element method.

Mass diffusion coefficient of air (m^2/s)		2.68E − 05
Channel	Length (mm)	210
	Wide (mm)	210
	Thickness (mm)	4
	Amount	123
Membrane	Thickness (mm)	0.05
	Heat conductivity coefficient (W/m/K)	0.1268
	Mass diffusion coefficient (m^2/s)	3.20E − 10
Exchanger size (mm)		1060 × 980 × 320
Core size (mm)		210 × 210 × 490
Inlet/outlet size (mm)		168 × 100

sensibility effectiveness increase along with the increase of airflow rate. Hence, the effective utilization rate of right area of MTHE core becomes progressively saturated as airflow rate increases.

2.5. Results and discussion of the theoretical model

Based on the description of the model in Fig. 3, the exchanger efficiencies of MTHE were also simulated with finite element method (FEM). In our work, the FEM software COMSOL 4.2a was used, the parameters used are listed in Table 2. Fig. 5 shows the cross-section average velocity distribution of inlet windward with core at 500 m^3/h. The ideal condition means the cross-section average velocity distribution of inlet windward with core is uniform, the simulation condition means it is simulation result with a MTHE construction such as Fig. 1.

For the simulation condition, the average velocity was much higher in the side close to inlet, with the maximum value appearing in the center of inlet (0.8 m). The minimum value appears on the edge of the inlet (0.5 m); and the average velocity in the left part

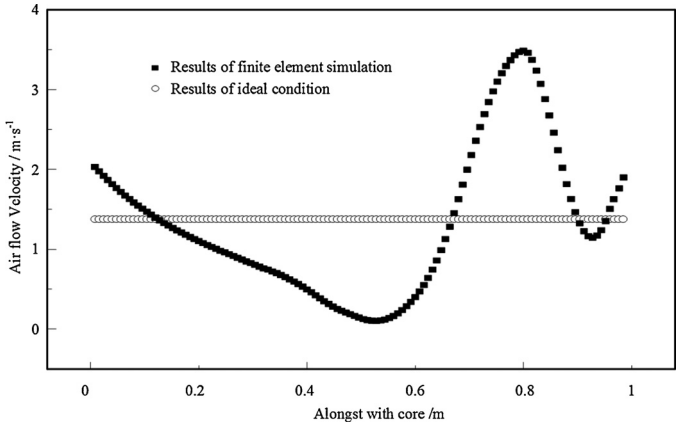

Fig. 5. Cross-section average velocity distribution of inlet windward with core.

(from 0 m to 0.5 m) was much lower than under ideal condition. Therefore, the latency and the sensibility effectiveness of MTHE in each channel are different because of various airflow velocities.

Simulation results indicate that the sensibility and the enthalpy effectiveness of each channel can be calculated. With the mean, the total sensibility and enthalpy effectiveness with each channel can be calculated by,

$$\eta_c = \frac{m_{c1} \times \eta_{c1} + m_{c2} \times \eta_{c2} + \cdots + m_{cn} \times \eta_{cn}}{m_{c1} + m_{c2} + \cdots + m_{cn}} \quad (14)$$

where $m_{c1} \ldots m_{cn}$ is the average mass flow rate of air of each channel; $\eta_{c1} \ldots \eta_{cn}$ is the exchange effectiveness of each channel; and n is the total number of channels. With Eq. (14), the mean values of the sensibility and of the enthalpy effectiveness of MTHE are 68.8% and 59.2%, respectively, and are 72.6% and 63.7%, respectively, under ideal conditions. Therefore, the non-uniform distribution of airflow has reduced the exchange effectiveness of MTHE. To describe the influence between uneven distribution of airflow and exchange effectiveness, a parameter was proposed as non-uniform coefficient (N) based on the variance theory of statistics. It indicates that the non-uniform of average airflow velocity distribution can be obtained by,

$$N = (m_{c1} - \overline{m})^2 + (m_{c2} - \overline{m})^2 + \cdots + (m_{cn} - \overline{m})^2, \quad \overline{m} = \frac{m_{c1} + m_{c2} + \cdots + m_{cn}}{n} \quad (15)$$

Fig. 6 shows the changes in non-uniform coefficient and the comparison of means of the sensibility and the enthalpy effectiveness between the actual and the ideal conditions against airflow rates. The non-uniform coefficient increases along with airflow rates. Meanwhile, with the increase of non-uniform coefficient, the difference between the exchange effectiveness of the actual and the ideal conditions likewise increased. Hence, the sensibility and the enthalpy effectiveness are influenced by the non-uniform distribution of airflow at windward.

3. Improved exchanger

With the aforementioned experiment and simulation analysis, an improved MTHE was proposed in this work (Fig. 7). The improved MTHE comprised the main and the blower tanks. The main tank consists of inlet, outlet, and core. The blower tank contains the flesh/exhaust air blower separated by a baffle. The inlet and the outlet sides were split into fresh air runner and exhaust air runner with air deflector by a horizontal baffle. On the fresh air and exhaust air runners of inlet, a certain number of air spreader plates were placed. The airflow can be uniformly distributed by adjusting the number or the construction of the air spreader plates. The process of airflow in the improved MTHE is shown in Fig. 8.

3.1. Experiment

The test rig described in Section 2.1 was used to verify the sensibility and the enthalpy effectiveness of the improved MTHE. The basic principles of the geometry of air spreader plates are:

(1) the arc tangential direction of the air spreader plates at core side should perpendicular to the inlet direction of core;
(2) the distribution of air spreader plates should be sure the inlet air equally distributed along the core.

As a comparison, the improved MTHEs with four different air spreader plates were selected. The geometry of air spreader plate was selected with FE simulation results, namely, (I) without air spreader plates, (II) with five equally divided air spreader plates

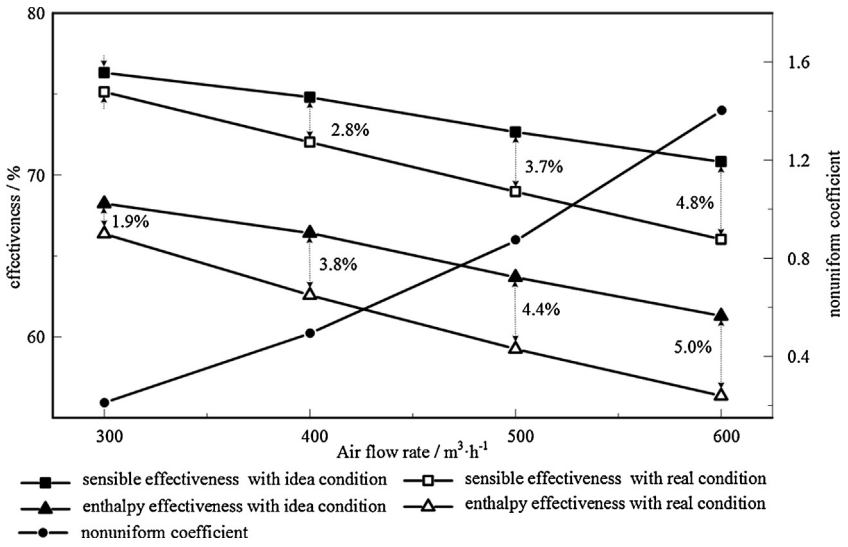

Fig. 6. Non-uniform coefficient and weighted mean of sensibility and enthalpy effectiveness.

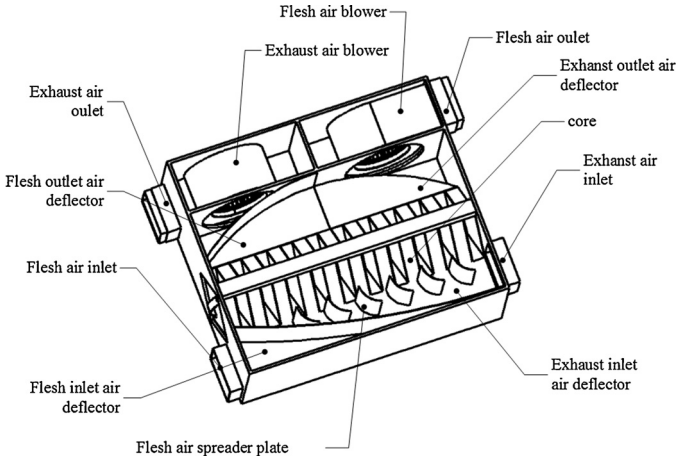

Fig. 7. Schematic of the improved MTHE.

(a = 7.6 cm, b = 10.7 cm, α = 70.8°), (III) with seven equally divided air spreader plates (a = 7.6 cm, b = 10.7 cm, α = 70.8°), (IV) with seven equally divided air spreader plates (a = 11 cm, b = 8.3 cm, α = 105.4°). The structure of air spreader plates is shown in Fig. 9.

3.2. Results and discussion

3.2.1. Effect of air deflector

The sensibility and the enthalpy effectiveness of the original MTHE described in Fig. 1 and the improved MTHE Type I were measured with the test rig. Results are shown in Fig. 10. For the original MTHE, as described in Fig. 5, most of the import fresh/exhaust air is concentrated in the fresh/exhaust inlet side of the core. Therefore, the change of sensibility and enthalpy effectiveness with airflow rate was insignificant. However, for the improved MTHE Type I, given the effect of air deflector, the airflow distribution was uniformed than the original MTHE at low airflow rate. Therefore, the sensibility and the enthalpy effectiveness were higher. As airflow rate increases, the airflow distribution becomes concentrated in the fresh/exhaust inlet side of the core because of airflow inertia. As a result, the reduction of effectiveness of Type I is significant (Figs. 10 and 11).

3.2.2. Effect of air spreader plates

In this paper, three different types of air spreader plates were placed in the air runner of Type I, namely, Types II–IV. The experimental results of the sensibility and the enthalpy effectiveness with test rig are shown in Figs. 10 and 11.

Comparing the test results of Types II and I, we noted that the sensibility and the enthalpy effectiveness had been improved, as well as the effectiveness is reduced along with decrease in airflow rate. However, the sensibility and the enthalpy effectiveness of Type II remain low than those of the original MTHE at high airflow rate. Therefore, the homogeneity of airflow distribution could be improved by the air spreader plates based on the results in Section 2.4. Given these analysis results above, a different MTHE was proposed as Type III with two more air spreader plates. Compared with the original MTHE, the sensibility and the enthalpy effectiveness of Type III have improved at 4.3% and 1.6% airflow rate, respectively. The sensibility and the enthalpy effectiveness can be improved

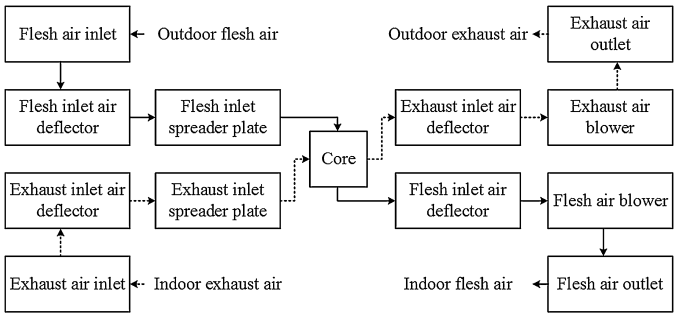

Fig. 8. Airflow process in the improved MTHE.

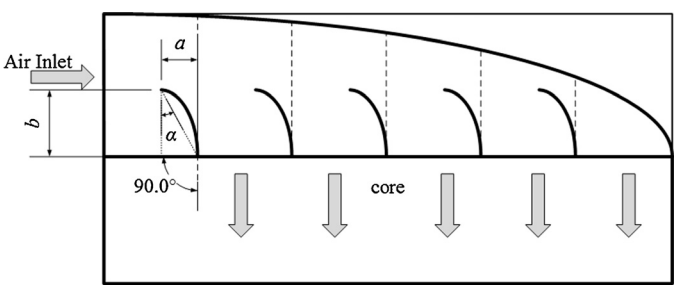

Fig. 9. Structure of air spreader plates.

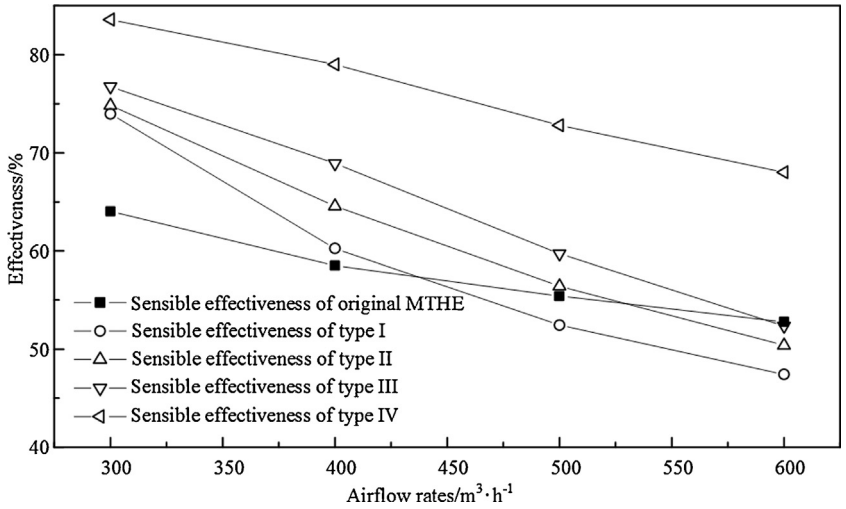

Fig. 10. Sensibility effectiveness of different types.

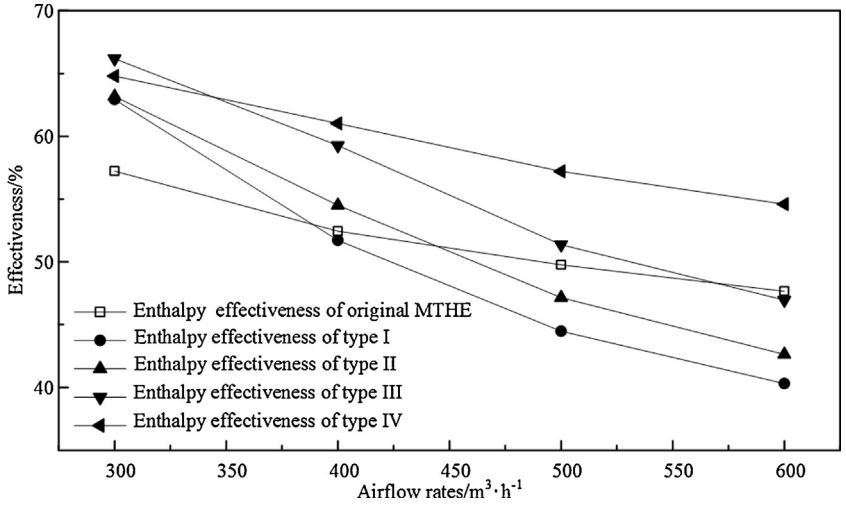

Fig. 11. Enthalpy effectiveness of different types.

by adding the quantity of air spreader plates. However, the effectiveness at high airflow rate remains unsatisfied. Therefore, differently shaped air spreader plate was used in Type IV with seven plates. Compared with the original MTHE, the sensibility and the enthalpy effectiveness of Type III have improved at 17.4% and 7.8% airflow rate, respectively. The angle α of air spreader plate in Fig. 9 was related with the effectiveness of MTHE.

4. Conclusion

In this work, with experimental method and FEM, the effect of the inlet airflow distribution was analyzed. With analyzed results, an improved MTHE with air deflectors and air spreader plates was proposed. Test rig was constructed to measure the sensibility and the enthalpy effectiveness of the improved MTHEs with different air spreader plates. With the improved MTHE, the sensibility and the enthalpy effectiveness have been optimized at 17.4% and 7.8% airflow rate, respectively.

Acknowledgement

The study was supported by National Natural Science Foundation of China (No. 51006116). The authors gratefully acknowledge them for financial support of this work.

References

[1] L.Z. Zhang, J.L. Niu, Effectiveness correlations for heat and moisture transfer processes in an enthalpy exchanger with membrane cores, Journal of Heat Transfer 124 (2002) 922–929 (T ASME).
[2] B.R. Baliga, R.R. Azrak, Laminar fully-developed flow and heat-transfer in triangular plate-fin ducts, Journal of Heat TransferV 108 (1986) 24–32 (T ASME).
[3] J. Liu, W. Li, J. Liu, B. Wang, Efficiency of energy recovery ventilator with various weathers and its energy saving performance in a residential apartment, Energy and Buildings 42 (2010) 43–49.
[4] J.L. Niu, L.Z. Zhang, Membrane-based enthalpy exchanger: material considerations and clarification of moisture resistance, Journal of Membrane Science 189 (2001) 179–191.
[5] L.Z. Zhang, Y. Jiang, Heat and mass transfer in a membrane-based energy recovery ventilator, Journal of Membrane Science 163 (1999) 29–38.
[6] Y. Fan, K. Kameishi, S. Onishi, K. Ito, Field-based study on the energy-saving effects of CO_2 demand controlled ventilation in an office with application of energy recovery ventilators, Energy and Buildings 68 (2014) 412–422.
[7] Y. Kang, Y. Wang, K. Zhong, J. Liu, Temperature ranges of the application of air-to-air heat recovery ventilator in supermarkets in winter, China, Energy and Buildings 42 (2010) 2289–2295.
[8] J. Zhang, A.S. Fung, S. Jhingan, Analysis and feasibility study of residential integrated heat and energy recovery ventilator with built-in economizer using an excel spreadsheet program, Energy and Buildings 75 (2014) 430–438.
[9] S-M. Kim, J-H. Lee, S. Kim, H.J. Moon, J. Cho, Determining operation schedules of heat recovery ventilators for optimum energy savings in high-rise residential buildings, Energy and Buildings 46 (2012) 3–13.
[10] L.Z. Zhang, Heat and mass transfer in plate-fin sinusoidal passages with vapor-permeable wall materials, International Journal of Heat and Mass Transfer 51 (2008) 618–629.

[11] J. Woods, E. Kozubal, Heat transfer and pressure drop in spacer-filled channels for membrane energy recovery ventilators, Applied Thermal Engineering 50 (2013) 868–876.
[12] B. Liu, J. Chen, X. Du, L. Xue, Poly(vinyl chloride)/montmorillonite hybrid membranes for total-heat recovery ventilation, Journal of Membrane Science 443 (2013) 83–92.
[13] E-J. Lee, J-P. Lee, N-H. Kim, Moisture transfer characteristics of a LiCl-impregnated paper membrane used for an enthalpy exchanger, Journal of Mechanical Science and Technology 27 (2013) 1527–1537.
[14] C.H. Lee, S.H. Kim, E.J. Son, T.H. Lim, Polypropylene melt blown nonwovens for plate-type enthalpy exchanger, Macromolecular Research 20 (2012) 4–9.
[15] L.Z. Zhang, Fabrication of a lithium chloride solution based composite supported liquid membrane and its moisture permeation analysis, Journal of Membrane Science 276 (2006) 91–100.
[16] J. Min, M. Su, Performance analysis of a membrane-based enthalpy exchanger: effects of the membrane properties on the exchanger performance, Journal of Membrane Science 348 (2010) 376–382.
[17] G. Ge, G.I. Mahmood, D.G. Moghaddam, C.J. Simonson, R.W. Besant, S. Hanson, et al., Material properties and measurements for semi-permeable membranes used in energy exchangers, Journal of Membrane Science 453 (2014) 328–336.
[18] L.Z. Zhang, X.R. Zhang, Q.Z. Miao, L.X. Pei, Selective permeation of moisture and VOCs through polymer membranes used in total heat exchangers for indoor air ventilation, Indoor Air 22 (2012) 321–330.
[19] J. Min, M. Su, Performance analysis of a membrane-based energy recovery ventilator: effects of membrane spacing and thickness on the ventilator performance, Applied Thermal Engineering 30 (2010) 991–997.
[20] J. Min, L. Wang, Coupled heat and mass transfer during moisture exchange across a membrane, Journal of Membrane Science 430 (2013) 150–157.
[21] J. Min, L. Wang, Heat of adsorption and its effects on transmembrane heat transfer, Journal of Membrane Science 409 (2012) 173–179.
[22] L. Wang, J. Min, Studies of the process of moisture exchange across a membrane using irreversible thermodynamics, Chinese Science Bulletin 56 (2011) 1836–1843.
[23] J. Woods, Membrane processes for heating, ventilation, and air conditioning, Renewable & Sustainable Energy Reviews 33 (2014) 290–304.
[24] L.-Z. Zhang, Progress on heat and moisture recovery with membranes: from fundamentals to engineering applications, Energy Conversion and Management 63 (2012) 173–195.
[25] J. Kragh, J. Rose, T.R. Nielsen, S. Svendsen, New counter flow heat exchanger designed for ventilation systems in cold climates, Energy and Buildings 39 (2007) 1151–1158.
[26] R. Al-Waked, M.S. Nasif, G. Morrison, M. Behnia, CFD simulation of air to air enthalpy heat exchanger, Energy Conversion and Management 74 (2013) 377–385.
[27] R. Pastor, Heat and Mass Transfer of a Countercurrent Flow Energy Recovery Ventilator (ERV), Rensselaer Polytechnic Institute, Hartford, CT, 2011.
[28] A. Mardiana-Idayu, S.B. Riffat, An experimental study on the performance of enthalpy recovery system for building applications, Energy and Buildings 43 (2011) 2533–2538.
[29] L-Z. Zhang, Heat and mass transfer in a quasi-counter flow membrane-based total heat exchanger, International Journal of Heat and Mass Transfer 53 (2010) 5478–5486.
[30] M. Nasif, R. Al-Waked, G. Morrison, M. Behnia, Membrane heat exchanger in HVAC energy recovery systems, systems energy analysis, Energy and Buildings 42 (2010) 1833–1840.